

## FRONTIERS ARTICLE

## Single-nanoparticle catalysis at single-turnover resolution

Peng Chen <sup>\*</sup>, Weilin Xu, Xiaochun Zhou, Debashis Panda, Aleksandr Kalininskiy

Department of Chemistry and Chemical Biology, Cornell University, Baker Laboratory, Ithaca, NY 14853, United States

## ARTICLE INFO

## Article history:

Received 7 January 2009

In final form 22 January 2009

Available online 27 January 2009

## ABSTRACT

Understanding the catalytic properties of nanoparticles is fundamentally important, but hampered by the intrinsic heterogeneity following from their structural dispersions and dynamics. This obstacle can be overcome if one can follow the catalysis of individual nanoparticles in real time. This article summarizes recent developments in using single-molecule fluorescence microscopy to study single nanoparticle catalysis. These studies reveal and quantify heterogeneous and dynamic behavior of individual nanoparticles that highlight the intricate interplay between catalysis, heterogeneous reactivity, variable surface sites, and surface restructuring dynamics in nanocatalysis. Challenges and future directions in single-nanoparticle catalysis research are also discussed.

© 2009 Elsevier B.V. All rights reserved.

## 1. Introduction

Nanoparticles of various materials can catalyze a multitude of chemical transformations for processing petroleum, oxidizing pollutants, and converting chemical energy to electricity [1–16]. Partly owing to their increased surface-to-volume ratio and new electronic properties from quantum confinement, nanoparticles often have new or superior catalytic activity, compared with their corresponding bulk materials [1–16]. The current global energy challenge has enhanced the enthusiasm in nanoparticle catalysts, as they are key components in photoelectrochemical cells and fuel cells [17]. To understand the fundamental principles governing their catalytic properties, intense efforts have thus been made to characterize the structure and the activity of nanoparticles.

On the structure side, nanoparticles can be studied *individually*, sometimes even *in situ*, down to atomic resolution with advanced transmission electron microscopy [4,10,11,13,14], scanning-probe microscopy [8,12], or X-ray diffraction [18]. On the activity side, in contrast, nanoparticles have been mainly studied *at the ensemble level*, obtaining their averaged catalytic properties. The ensemble-averaged characterization is fundamentally inadequate, however, owing to the intrinsic activity heterogeneity of nanoparticles that arises from their two characteristics: First, there is always structural dispersion among a population of nanoparticles, with different sizes and shapes; even for a single nanoparticle, its surface has a variable distribution of atoms on corners, edges, and facets [4,19,20]. Do these nanoparticles have identical activity then? The answer is expectedly 'no'. But, more important, how different are they, and can we correlate the distribution of their structure with that of their activity? Second, the structures of nanoparticles, especially on their surfaces, are dynamic during catalysis; large

morphology changes and surface restructuring can occur because of constantly changing adsorbate–surface interactions in catalysis [1,4,14,15,20–24]. These structural changes will cause temporal activity fluctuations that are asynchronous among the nanoparticles. How do we then think about the temporal behaviors of nanoparticle catalysis?

To address the above questions, one needs to study nanoparticle catalysis at the single-particle level in real time, preferably with single-turnover resolution. A few research groups have reported electrochemistry measurements on a single nanoelectrode or nanoparticle by detecting electric currents [25–30]. Using surface plasmon spectroscopy, Novo et al. observed the steady-state accumulation of redox reactions catalyzed by single Au nanocrystals [31]. Nevertheless, how heterogeneous the nanoparticle activities are and how individual nanoparticles behave temporally remain to be elucidated.

Our group recently reported a single-molecule approach to study nanoparticle catalysis at the single-particle level [32–34]. We used single-molecule microscopy of fluorogenic reactions, a strategy started in single-enzyme studies [35–38], and later applied as well to microcrystal catalysts [39]. In this approach, we detect the fluorescence of a catalytic product at the single-molecule level to monitor redox catalysis by individual Au nanoparticles at single-turnover resolution under ambient conditions. In this article, we review the methodology, the results, and the information content of the single-molecule study of nanocatalysis; we also discuss the challenges and provide an outlook to the future developments.

## 2. Single-molecule fluorescence approach to nanocatalysis

Our approach is based on the single-molecule detection of fluorogenic reactions. We discovered that colloidal Au nanoparticles

<sup>\*</sup> Corresponding author. Fax: +1 607 255 4137.

E-mail address: [pc252@cornell.edu](mailto:pc252@cornell.edu) (P. Chen).

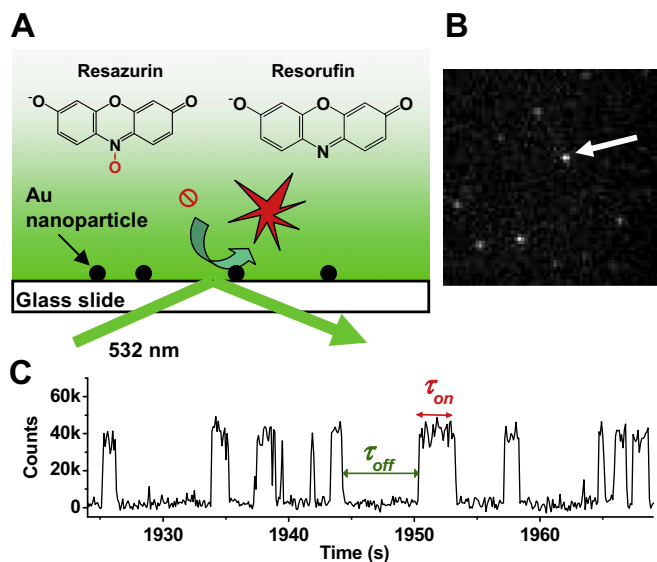


**Fig. 1.** Single-turnover detection of single Au nanoparticle catalysis. (A) Experimental design using total internal reflection fluorescence microscopy with 532-nm laser excitation. (B) Typical image ( $\sim 18 \times 18 \mu\text{m}^2$ ) of fluorescent products during catalysis by 6-nm Au-nanoparticles. (C) Segment of the fluorescence trajectory from the fluorescence spot marked by the arrow in B. Figures adapted from Ref. [32].

catalyze the fluorogenic reduction of nonfluorescent resazurin to highly fluorescent resorufin by  $\text{NH}_2\text{OH}$  in aqueous solutions [32]. These colloidal Au nanoparticles are prepared from citrate reduction of  $\text{HAuCl}_4$  in aqueous solutions [40,41], and their surfaces have adsorbed citrate ions making them negatively charged and stabilized as colloids. Fig. 1A depicts our experimental design using total internal reflection fluorescence microscopy. Au nanoparticles are immobilized on an amine-coated, positively charged glass surface at low density so individual nanoparticles are separated spatially by micrometer scale. The nonfluorescent substrate resazurin and the reductant  $\text{NH}_2\text{OH}$  are kept in a flowing solution above. Each reaction catalyzed by a Au nanoparticle produces a fluorescent product resorufin on the nanoparticle surface. This product molecule emits hundreds or more of fluorescence photons under laser excitation before it dissociates from the nanoparticle and becomes undetectable because of its fast diffusion in solution. At the single-molecule imaging condition, the catalysis gives out *stochastic bursts* of fluorescence signals at *localized spots* on the glass slide where individual Au nanoparticles reside; each burst of fluorescence is one product, i.e., one turnover, catalyzed by a single Au nanoparticle. Fig. 1B shows a typical fluorescence image of catalysis by 6-nm spherical Au-nanoparticles; the image contains localized, discrete fluorescence spots of diffraction-limited size ( $\sim 300$  nm in width).

A typical time trajectory of fluorescence intensity from one of these fluorescence spots contains stochastic off–on signals (Fig. 1C). The digital nature of the trajectory and the consistent height of the on-level are characteristic of single-molecule fluorescence detection. Each sudden intensity increase in the trajectory marks a product formation on the nanoparticle; each decrease marks a product dissociation from the nanoparticle; and each off–on cycle corresponds to a single-turnover of a catalytic formation of a product on one nanoparticle and its subsequent dissociation. The actual chemical transformations of catalysis and dissociation occur on the sub-picosecond timescale and are irresolvable in single-molecule fluorescence measurements.

Because the reaction products are continuously generated, such experiments can monitor reactions of a single Au nanoparticle for extended time without the limit of fluorescence photobleaching. With these real-time turnover trajectories of single nanoparticles,

one can: (1) Determine the reaction rate (i.e., activity) of a single nanoparticle. (2) Determine the kinetic mechanism of the catalyzed reaction. (3) Obtain the distribution of the catalytic properties of nanoparticles. (4) Analyze the temporal dynamics of the turnover events of a single nanoparticle. In the following, we discuss the information content in these single-particle turnover trajectories and their quantitative analyses, focusing on the results of 6-nm spherical Au nanoparticles.

### 3. Information content

#### 3.1. Direct observation of multiple active sites

The single-molecule approach to nanocatalysis can directly observe the multiplicity of active sites on the surface of a single Au nanoparticle. In some single-particle turnover trajectories, the fluorescence bursts occasionally show multiple on-levels (Fig. 2). These multi-level events indicate that a new resorufin product is generated on the nanoparticle surface before earlier ones dissociate away, and therefore, directly reflect the multitude of either catalytic sites that can exhibit parallel catalysis, or docking sites where products can stay on the Au nanoparticle surface before dissociation. For the Au nanoparticles studied here, both catalytic sites and product docking sites are present (see Section 3.6).

#### 3.2. Kinetic mechanism of catalysis

In the single-particle turnover trajectories (Fig. 1C), the actual events of catalytic product formation or product dissociation are irresolvable and appear as sudden intensity jumps. However, the time needed (the ‘waiting time’) for substrate diffusion, binding, or thermal activation before such an event is usually much longer. The  $\tau_{\text{off}}$  and  $\tau_{\text{on}}$  are the two waiting times and the most important observables in these turnover trajectories. Resolving them enables the analysis of the kinetic mechanism in two parts separately:  $\tau_{\text{off}}$  is the waiting time before each product formation, and  $\tau_{\text{on}}$  is the waiting time for product dissociation after its formation. The individual values of  $\tau_{\text{off}}$  and  $\tau_{\text{on}}$  are stochastic, but their statistical properties, such as average values and distributions, are defined by the underlying reaction kinetics, and thus report the kinetic mechanism of the catalysis.

To simplify the kinetics and to focus on the resazurin reduction, we performed all catalysis experiments under a saturating  $\text{NH}_2\text{OH}$  concentration, so the explicit term for  $\text{NH}_2\text{OH}$  can be omitted from the kinetic mechanism. Under this condition, the catalytic conversion reaction of resazurin to resorufin, which is contained in  $\tau_{\text{off}}$ , follows the Langmuir–Hinshelwood mechanism for heterogeneous catalysis [42] – the nanoparticle catalyzes the conversion of the substrate resazurin to the product resorufin while maintaining a fast substrate adsorption equilibrium (Fig. 3A, reaction (i)); the number of adsorbed substrate molecules follows the Langmuir adsorption isotherm. This kinetic mechanism is reflected by the resazurin concentration ( $[S]$ ) dependence of  $\langle \tau_{\text{off}} \rangle^{-1}$  ( $\langle \rangle$  denotes

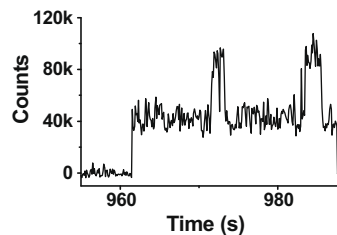


**Fig. 2.** Segment of a fluorescence turnover trajectory of a 6-nm Au nanoparticle showing two on-levels. Figure taken from Ref. [32].

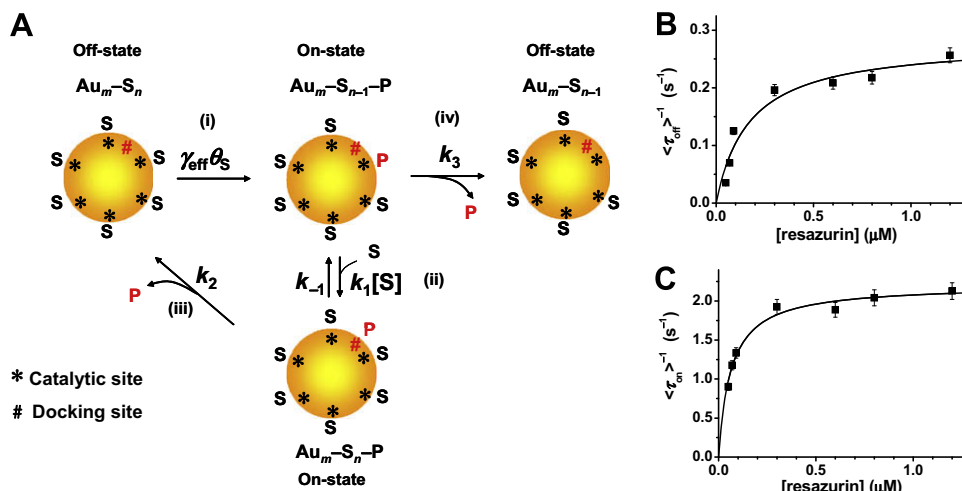


**Fig. 3.** Kinetic mechanism of catalysis. (A) Schematic of the kinetic mechanism.  $\text{Au}_m$ : Au-nanoparticle; S: resazurin; P: resorufin.  $\text{Au}_m\text{-S}_n$  represents a Au nanoparticle having  $n$  adsorbed substrate molecules at adsorption equilibrium. The fluorescence state (on or off) of the nanoparticle is indicated at each reaction stage. (B and C) Resazurin concentration dependence of  $\langle \tau_{\text{off}} \rangle^{-1}$  and  $\langle \tau_{\text{on}} \rangle^{-1}$ . Data here are averaged over many Au nanoparticles. Solid lines are fits with Eqs. (1) and (2) with  $\gamma_{\text{eff}} = 0.28 \text{ s}^{-1}$ ,  $K_1 = 6 \mu\text{M}^{-1}$ ,  $k_2 = 2.2 \text{ s}^{-1}$ ,  $K_2 = 16 \mu\text{M}^{-1}$ , and  $k_3 = 0 \text{ s}^{-1}$ . Note here the values of the kinetic parameters are the average of many nanoparticles. Figures taken from Ref. [32].

averaging), which represents the time-averaged single-particle rate of product formation. With increasing  $[S]$ ,  $\langle \tau_{\text{off}} \rangle^{-1}$  exhibits saturation kinetics (Fig. 3B); this dependence is described quantitatively by the single-molecule Langmuir–Hinshelwood equation [32,33]:

$$\langle \tau_{\text{off}} \rangle^{-1} = \frac{1}{\int_0^{\infty} \tau f_{\text{off}}(\tau) d\tau} = kn_T \theta_S = \frac{\gamma_{\text{eff}} K_1 [S]}{1 + K_1 [S]}. \quad (1)$$

Here  $f_{\text{off}}(\tau)$  is the probability density function of  $\tau_{\text{off}}$ ;  $k$  is the catalytic rate constant for one catalytic site;  $n_T$  is the total number of surface catalytic sites on one Au nanoparticle;  $\theta_S$  is the fraction of substrate-occupied catalytic sites;  $K_1$  is the substrate adsorption equilibrium constant; and  $\gamma_{\text{eff}} = kn_T$ , representing the combined reactivity of all surface catalytic sites on one Au nanoparticle. In the  $\langle \tau_{\text{off}} \rangle^{-1}$  versus  $[S]$  curve (Fig. 3B), the saturation level and initial slope are  $\gamma_{\text{eff}}$  and  $\gamma_{\text{eff}} K_1$ , respectively.

On a related note, the single-molecule Langmuir–Hinshelwood equation explicitly includes the multiplicity of catalytic sites. This feature is advantageous, as well as makes it applicable, for treating single-molecule kinetics of oligomeric enzymes that contain multiple catalytic sites, as compared with the single-molecule Michaelis–Menten equation, which uses a one-site, one-substrate model [33,43].

For the dissociation of the product resorufin, which is contained in  $\tau_{\text{on}}$ , the reaction kinetics includes two parallel reaction pathways: one a substrate-assisted product dissociation pathway, in which the nanoparticle binds a substrate first before the product leaves the particle surface (Fig. 3A, reactions (ii) and (iii)), and the other a direct dissociation pathway (Fig. 3A, reaction (iv)). The substrate-assisted dissociation pathway is reflected by the  $[S]$  dependence of  $\langle \tau_{\text{on}} \rangle^{-1}$ , the time-averaged single-particle rate of product dissociation – with increasing  $[S]$ ,  $\langle \tau_{\text{on}} \rangle^{-1}$  increases and eventually saturates (Fig. 3C). The direct dissociation pathway is reflected by the value of  $\langle \tau_{\text{on}} \rangle^{-1}$  at  $[S] \rightarrow 0$ . The equation that quantifies the overall  $[S]$  dependence of  $\langle \tau_{\text{on}} \rangle^{-1}$  is:

$$\langle \tau_{\text{on}} \rangle^{-1} = \frac{1}{\int_0^{\infty} \tau f_{\text{on}}(\tau) d\tau} = \frac{k_2 K_2 [S] + k_3}{1 + K_2 [S]}. \quad (2)$$

Here  $f_{\text{on}}(\tau)$  is the probability density function of  $\tau_{\text{on}}$ ,  $k_2$  is the rate constant of product dissociation in the substrate-assisted pathway (reaction (iii)),  $k_3$  is the rate constant of direct product dissociation (reaction (iv)), and  $K_2 = k_1/(k_{-1} + k_2)$  (Fig. 3A).  $k_3$ , the rate constant

for the direct dissociation pathway is irresolvable when the data are averaged over many Au nanoparticles (Fig. 3C), but it is clearly identifiable when looking at  $\langle \tau_{\text{on}} \rangle^{-1}$  versus  $[S]$  for a single particle (see Section 3.4).

### 3.3. Heterogeneity in catalytic reactivity

The structural dispersion among nanoparticles suggests that individual nanoparticles should have different reactivity, but quantifying just how different they are has been challenging. Single-particle measurements can directly examine and quantify the heterogeneity in catalytic reactivity of Au nanoparticles. On a single-particle basis, Eq. (1) predicts the catalytic product formation rate  $\langle \tau_{\text{off}} \rangle^{-1}$  to show variable saturation levels and initial slopes, if different Au nanoparticles have heterogeneous catalytic reactivity ( $\gamma_{\text{eff}}$ ) and substrate binding affinity ( $K_1$ ). Experimentally, different nanoparticles indeed show distinct saturation levels and initial slopes in their  $\langle \tau_{\text{off}} \rangle^{-1}$  versus  $[S]$  titration curves (Fig. 4A); from these curves,  $\gamma_{\text{eff}}$  and  $K_1$  of each nanoparticle can be extracted.

Alternatively,  $\gamma_{\text{eff}}$  can be obtained from the distribution of the  $\tau_{\text{off}}$  from a single-particle turnover trajectory. At saturating resazurin concentrations (i.e.,  $[S] > 1 \mu\text{M}$  for the 6-nm Au nanoparticles), all nanoparticle surface catalytic sites are occupied by substrates, and  $f_{\text{off}}(\tau)$ , the probability density function of  $\tau_{\text{off}}$ , is related to the kinetic parameters as  $f_{\text{off}}(\tau) = \gamma_{\text{eff}} \exp(-\gamma_{\text{eff}} \tau)$  [32,33]. Therefore,

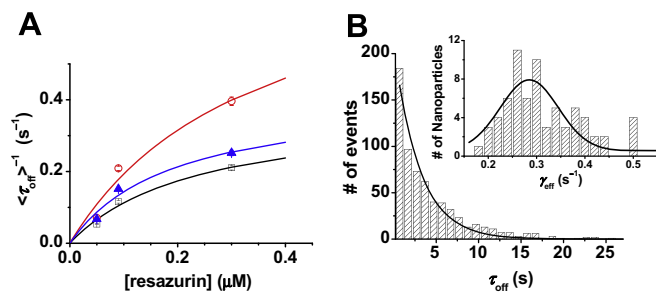


**Fig. 4.** Heterogeneity in catalytic reactivity. (A) Resazurin concentration dependence of  $\langle \tau_{\text{off}} \rangle^{-1}$  from three Au nanoparticles. Solid lines are fits with Eq. (1). (B) Distributions of  $\tau_{\text{off}}$  from a single trajectory at a saturating  $[S]$ . Solid line is a single-exponential fit with  $\gamma_{\text{eff}} = 0.33 \text{ s}^{-1}$ . Inset: distribution of  $\gamma_{\text{off}}$  from many Au nanoparticles; solid line is a Gaussian fit. Figures taken from Refs. [32,34].

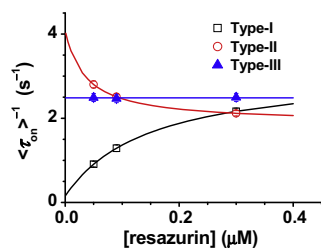


**Fig. 5.** Differential selectivity between parallel reaction pathways. Resazurin concentration dependence of  $\langle \tau_{\text{on}} \rangle^{-1}$  from three Au nanoparticles of type-I, type-II, and type-III. Solid lines are fits with Eq. (2): for the type-I nanoparticle,  $k_2 = 3.2 \text{ s}^{-1}$ ,  $K_2 = 6.7 \text{ } \mu\text{M}^{-1}$ , and  $k_3 = 0.15 \text{ s}^{-1}$ ; for the type-II,  $k_2 = 1.8 \text{ s}^{-1}$ ,  $K_2 = 28 \text{ } \mu\text{M}^{-1}$ , and  $k_3 = 4.1 \text{ s}^{-1}$ ; for the type-III,  $k_2 = k_3 = 2.4 \text{ s}^{-1}$  (or  $k_2 = 0$ ), and  $K_2 = \text{arbitrary value}$ . Figure adapted from Ref. [32].

fitting the distribution of  $\tau_{\text{off}}$  from a single-particle trajectory with an exponential function gives  $\gamma_{\text{eff}}$  directly (Fig. 4B); here the large number of turnover events in a single trajectory also ensures the statistical accuracy of the value of  $\gamma_{\text{eff}}$ . From analyzing many single-particle trajectories, we can obtain the distribution of  $\gamma_{\text{eff}}$  (Fig. 4B, inset). The broad distribution of  $\gamma_{\text{eff}}$  quantifies the heterogeneity in catalytic reactivity of the Au nanoparticles.

### 3.4. Differential selectivity between parallel reaction pathways

In the kinetic mechanism (Fig. 3A), the product dissociation process contains two parallel reaction pathways: one a substrate-assisted pathway and the other a direct dissociation pathway. For a single Au nanoparticle, these parallel pathways immediately pose a fascinating problem: how is a single nanoparticle going to choose between the two pathways? Does it prefer one to the other, or take the two pathways equally? The kinetics of a single Au nanoparticle will report its differential selectivity between parallel reaction pathways.

Experimentally, the differential selectivity of a single Au nanoparticle in the product dissociation reaction is manifested by the [S] dependence of its  $\langle \tau_{\text{on}} \rangle^{-1}$ . From Eq. (2), when  $[S] \rightarrow 0$ ,  $\langle \tau_{\text{on}} \rangle^{-1} = k_3$ , i.e., the direct dissociation dominates; when  $[S] \rightarrow \infty$ ,  $\langle \tau_{\text{on}} \rangle^{-1} = k_2$ , i.e., the high [S] drives the product dissociation to the substrate-assisted pathway. If  $k_2$  and  $k_3$ , the product dissociation rate constants in the two pathways, differ in their relative magnitudes,  $\langle \tau_{\text{on}} \rangle^{-1}$  will have three types of kinetic behaviors: (I) asymptotic increase with increasing [S] if the nanoparticle has  $k_2 > k_3$ , i.e., the nanoparticle prefers the substrate-assisted dissociation pathway; (II) asymptotic decrease if  $k_2 < k_3$ , i.e., the nanoparticle prefers the direct dissociation pathway; and (III) constant at any [S] if  $k_2 = k_3$ , i.e., the nanoparticle takes the two pathways equally, or if  $K_2 = 0$ . All three types of kinetic behaviors are observed, and they have different subpopulations (Fig. 5): 66% of Au nanoparticles are type-I, 19% are type-II, and 15% are type-III. This differential selectivity between parallel reaction pathways is completely hidden in ensemble-averaged measurements, in which type-I nanoparticles dominate and the direct dissociation pathway is unidentifiable (Fig. 3C).

### 3.5. Nanoparticles as dynamic entities: temporal catalytic dynamics

Owing to their nanometer dimensions, nanoparticle surfaces are unstable and can reconstruct dynamically [1,4,14,15,20–24], especially under catalysis, where the constantly changing adsorbate–surface interactions can induce dynamic surface reconstruction. This long-envisioned dynamic nature of nanoparticle surface structure has recently been observed directly with advanced techniques [14,15,19–22,24,44]. These structural dynamics will inevitably cause temporal dynamics of catalytic activity, termed

‘dynamic disorder’ in chemical kinetics. This dynamic disorder is extremely challenging to study in ensemble measurements, especially because the temporal dynamics of individual particles are asynchronous. Here, the real-time single-particle measurements offer direct probing of temporal catalytic dynamics.

From each single-particle turnover trajectory, we can determine the time-dependence of the rate of turnovers (Fig. 6A). Large temporal fluctuations are clearly observable, indicating dynamic activity fluctuations of single Au nanoparticles. These activity fluctuations have contributions from the reaction rate changes both in the  $\tau_{\text{off}}$  reaction (the catalytic product formation) and in the  $\tau_{\text{on}}$  reaction (the product dissociation). These two contributions can be evaluated separately for each particle by extracting the sequences of individual  $\tau_{\text{off}}$  and  $\tau_{\text{on}}$  from the turnover trajectory and analyzing their autocorrelation functions  $C_{\tau}(m) = \langle \Delta\tau(0)\Delta\tau(m) \rangle / \langle \Delta\tau^2 \rangle$  [45,46]. Here,  $\tau$  is either  $\tau_{\text{off}}$  or  $\tau_{\text{on}}$ ,  $m$  is the turnover index number in the sequences, and  $\Delta\tau(m) = \tau(m) - \langle \tau \rangle$ . The exponential decay behaviors of  $C_{\tau_{\text{off}}}(m)$  and  $C_{\tau_{\text{on}}}(m)$  directly manifest the activity fluctuations in both the catalytic product formation and the product dissociation reactions (Fig. 6B and C). And the decay constants of  $C_{\tau_{\text{off}}}(m)$  and  $C_{\tau_{\text{on}}}(m)$  give the fluctuation correlation times that are also the timescales of the underlying surface restructuring dynamics. Moreover, different Au nanoparticles have very different activity fluctuation timescales, reflected in the broad distributions of the fluctuation correlation times from many Au nanoparticles (Fig. 6B and C, insets).

The catalysis-induced nature of the activity fluctuations and the underlying surface restructuring are directly supported by the positive correlation between the activity fluctuation rates, i.e., the inverse of the correlation times, and the rate of turnovers – for all Au nanoparticles, the activity fluctuation rates increase with increasing rates of turnovers (Fig. 7). The fluctuation rates can be further extrapolated linearly to zero rate of turnovers. The positive intercepts approximate the rates of spontaneous (as compared with catalysis-induced) surface restructuring dynamics for a Au nanoparticle in an aqueous environment, corresponding to a timescale of 40–150 s. The determination of a timescale for nanoparticle surface restructuring dynamics in the absence of catalysis is exciting, because it is directly related to the energetics of nanoparticle surface atoms and because they are in general challenging to quantify, owing to the nanometer dimension and the heterogeneous surface structure of nanoparticles.

### 3.6. Differentiation between surface catalytic and docking sites

The activity fluctuation rates of the  $\tau_{\text{off}}$  and the  $\tau_{\text{on}}$  reactions show a clear difference at the highest rate of turnovers (Fig. 7), where, owing to high [S],  $\gamma_{\text{eff}}$  and  $k_2$  dominate the  $\tau_{\text{off}}$  and  $\tau_{\text{on}}$  reactions, respectively (reference Eqs. (1) and (2)). This difference indicates that  $\gamma_{\text{eff}}$  and  $k_2$  experience distinct surface restructuring dynamics. Therefore, on each nanoparticle, the catalytic sites, where the catalytic reaction  $\gamma_{\text{eff}}$  occurs, are different from the docking sites, where the dissociation reaction  $k_2$  occurs (Fig. 3A).

The distinction between the catalytic sites and the docking sites is further supported by the correlations between the kinetic parameters for each nanoparticle. No significant correlation is observed between  $\gamma_{\text{eff}}$  and  $k_2$  for individual Au nanoparticles, with their correlation coefficient  $\rho_{\gamma_{\text{eff}},k_2} \sim 0.0$  (Fig. 8A).<sup>1</sup> As for  $k_3$ , the direct product dissociation reaction, it occurs at the same surface site as that of  $\gamma_{\text{eff}}$  (Fig. 3A); consistently, significant correlation is ob-

<sup>1</sup> The correlation coefficient  $\rho_{x,y}$  between two variables  $x$ ,  $y$  is defined as  $\rho_{x,y} = \langle (xy) \rangle - \langle x \rangle \langle y \rangle / \sqrt{(\langle x^2 \rangle - \langle x \rangle^2)(\langle y^2 \rangle - \langle y \rangle^2)}$ , where  $\langle \rangle$  denotes averaging. The value of  $\rho_{x,y}$  is between  $-1$  and  $1$ : if  $x$  and  $y$  are completely correlated,  $\rho_{x,y} = 1$ ; if completely uncorrelated,  $\rho_{x,y} = 0$ ; and if completely anticorrelated,  $\rho_{x,y} = -1$ .

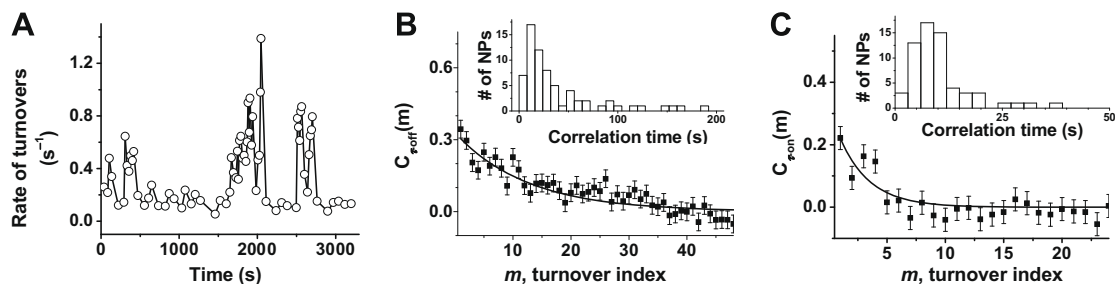


**Fig. 6.** Single-nanoparticle catalytic dynamics. (A) Trajectory of rate of turnovers for a single Au nanoparticle at a saturating substrate concentration. (B and C) Autocorrelation functions of  $\tau_{\text{off}}$  and  $\tau_{\text{on}}$  derived from the same turnover trajectory as that in A. Solid lines are exponential fits with decay constants of  $m_{\text{off}} = 12.5 \pm 2.9$  and  $m_{\text{on}} = 2.6 \pm 0.9$  turnovers. Insets: histograms of fluctuation correlation times for  $\tau_{\text{off}}$  and  $\tau_{\text{on}}$  reactions at a saturating substrate concentration. The fluctuation correlation times are obtained from the decay constants  $m_{\text{off}}$  and  $m_{\text{on}}$  multiplied by the average turnover time. NPs: nanoparticles. Figures adapted from Ref. [32].

served between  $\gamma_{\text{eff}}$  and  $k_3$  ( $\rho_{\gamma_{\text{eff}}, k_3} \sim 0.4$ , Fig. 8B), but not between  $k_2$  and  $k_3$  ( $\rho_{k_2, k_3} \sim 0.1$ , Fig. 8C). These correlations between kinetic rate constants further corroborate the kinetic mechanism for Au nanoparticle catalysis in Fig. 3A.

The distinction between the catalytic and docking sites also provides hints on the nature of the activity differences among type-I, II, and III nanoparticles, which differ in their relative magnitudes of  $k_2$  and  $k_3$  (Fig. 5). The direct product dissociation reaction  $k_3$  occurs from the catalytic sites, as compared with the docking sites for  $k_2$  (Fig. 3A). Therefore, the different activities of the three types of nanoparticles reflect the different properties (possibly slightly different structures) of their surface catalytic sites and product docking sites.

### 3.7. [S]-dependent dynamic surface switching

Owing to adsorbate–surface interactions and potential adsorbate–adsorbate interactions, catalytic properties of solid surfaces are dependent on the concentration of reactant molecules on the surface and in the reaction medium. For the Au nanoparticles, our single-particle single-turnover measurements revealed their [S]-dependent surface catalytic behaviors, showing abrupt switching between a low catalytic reactivity and a high reactivity state at a certain substrate concentration [34].

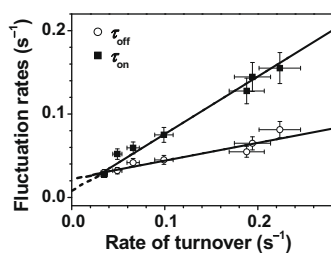


**Fig. 7.** Dependence of the activity fluctuation rate (i.e., the inverse of fluctuation correlation time) on the rate of turnovers. Figure adapted from Ref. [32].

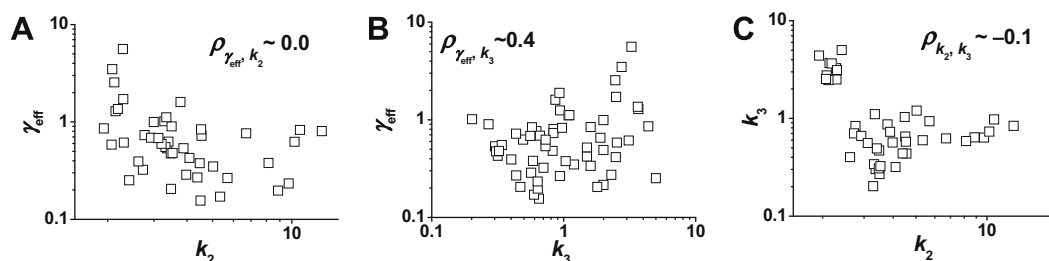


**Fig. 8.** Scattered plots in log-log scale and cross correlations between  $\gamma_{\text{eff}}$  and  $k_2$  (A), between  $\gamma_{\text{eff}}$  and  $k_3$  (B), and between  $k_3$  and  $k_2$  (C) for individual Au nanoparticles. Figures taken from Ref. [34].

We discovered this [S]-dependent dynamic surface switching by analyzing the variances (Var) of individual  $\tau_{\text{off}}^{-1}$  and  $\tau_{\text{on}}^{-1}$  from each turnover trajectory. These variances quantify the amplitudes of the time-dependent fluctuations of  $\tau_{\text{off}}^{-1}$  and  $\tau_{\text{on}}^{-1}$  of a single Au nanoparticle. At a low [S], the two-dimensional histogram of  $\text{Var}(\tau_{\text{off}}^{-1})$  and  $\text{Var}(\tau_{\text{on}}^{-1})$  of many Au nanoparticles shows a single population (type-a, Fig. 9A). With increasing [S], part of the type-a population switch to another distinct population at larger  $\text{Var}(\tau_{\text{off}}^{-1})$  and  $\text{Var}(\tau_{\text{on}}^{-1})$  (type-b, Fig. 9B). With further increase in [S], all type-a switch to type-b (Fig. 9C). Analyzing the type-a and type-b populations separately show that type-a has lower catalytic reactivity with stronger substrate binding and type-b has higher reactivity with weaker substrate binding [34].

The absence of intermediate behavior indicates that the two types of surface behaviors do not contribute simultaneously; for each Au nanoparticle, it can either behave as type-a or type-b and switches at a certain critical concentration. The switching concentration also varies largely from particle to particle, spanning a concentration range of two orders of magnitude (Fig. 10). Most Au nanoparticles switch around  $0.07 \mu\text{M}$  resazurin, while some of them switch at as low as  $\sim 0.02 \mu\text{M}$  or as high as  $\sim 1 \mu\text{M}$  resazurin.

We do not yet know the molecular detail of the dynamic switching of Au nanoparticle surface behaviors. It could come from surface reconstruction induced by substrate adsorption and catalysis, or adsorption reorientation of substrate on the particle surface, or substrate–substrate interactions. But in any case, the underlying process must be cooperative, i.e., having high-order kinetics on substrate concentration, to behave like a switch.

The dependence of surface catalytic behaviors on substrate concentration has strong implications in experimental studies of nanoparticle catalysts, or heterogeneous catalysts in general. It makes imperative to study heterogeneous catalysis at conditions relevant to real applications. Ultrahigh vacuum studies, for which many powerful spectroscopic techniques are available to provide rich information on catalytic mechanisms, should be complemented with high pressure, high concentration studies (e.g., in solution),

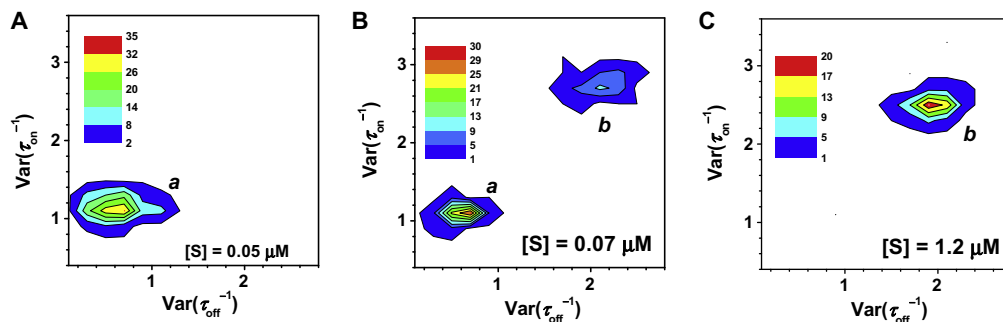


**Fig. 9.** [S]-dependent dynamic surface switching. Two-dimensional histograms of the variances of  $\tau_{\text{off}}^{-1}$  and  $\tau_{\text{on}}^{-1}$  of individual Au nanoparticles at different resazurin concentrations. Figures taken from Ref. [34].

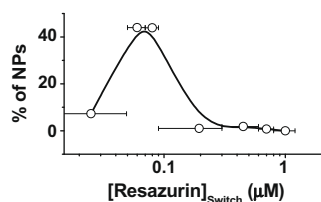


**Fig. 10.** Population distribution (%) of the Au-nanoparticles across different type-a-to-b switching concentrations. Figure adapted from Ref. [34].

to gain a full understanding of the catalytic properties [47–49]; and for nanoparticles, single-particle resolution is necessary.

#### 4. Challenges and outlook

For the inherently heterogeneous nanoparticle catalysts, the single-molecule fluorescence approach provides a powerful way to interrogate the intricate interplay between the catalytic activity, heterogeneous reactivity, and dynamic surface properties of individual nanoparticles. For the Au nanoparticles discussed here, the single-molecule studies have revealed and quantified their heterogeneous reactivity in catalysis, differential selectivity between parallel reaction pathways, surface-restructuring-coupled catalytic dynamics, and dynamic surface switching; much of this information lies beyond the reach of conventional ensemble measurements. Nevertheless, many questions remain to be answered. For example, what is the structural basis of the activity heterogeneity? Why do different nanoparticles show differential selectivity? Can we directly visualize the surface restructuring dynamics of a nanoparticle in real time? What is the physical basis of the substrate concentration dependent surface switching?

To answer above questions, one can study how the activity, heterogeneity, and dynamics of nanoparticles vary with their size and shape at the single-particle level. By varying their size and shape systematically, which changes the surface atom distributions over corners, edges, and facets [4,10,50–52], one may learn how specific surface structures contribute to the nanoparticle catalytic properties. Ultimately, one needs to bring together the activity measurements and the structural measurements onto individual nanoparticles, to directly correlate the activity of a single nanoparticle to its structure. Many high-resolution imaging methods, such as transmission electron microscopy and scanning tunneling microscopy, are available to examine nanoparticle structure down to atomic resolution; integrating them with single-particle catalysis measurements will surely generate unprecedented insights into the fundamental structure-activity relations of nanoparticle catalysts.

The single-molecule fluorescence approach, although powerful, does not come without limitations. Owing to the nanosecond pho-

ton-emission rate limited by the fluorescence lifetime, single-molecule fluorescence measurements have, at best,  $\mu\text{s}$  time resolution. The actual chemical transformations, occurring at sub-picosecond timescale, are thus irresolvable. Furthermore, fluorescence contains limited chemical information about the molecule; single-molecule detection via surface enhanced Raman scattering (SERS) can be a complementary and powerful approach [53–56].

As this approach is based on fluorescence detection, one of the products needs to be fluorescent, and catalytic reactions involving small molecules, such as methanol oxidation or water splitting, cannot be studied directly. The types of catalytic transformations to be studied are not limited, however, as one can create reactant molecules that undergo the desired chemical transformation to generate a fluorescence molecule. For example, if dehydrogenation reaction of C–C bond is of interest, one can design a molecule that if dehydrogenated, the resulted double bond completes an extended conjugation, forming a fluorescent product. With creative synthetic chemistry to generate suitable fluorogenic probes, many nanoparticle catalysts can be studied, either as isolated colloidal particles or on catalyst supports. Besides chemical catalysis, the approach can be easily extended to study electrocatalysis, wherein electrodes are used to supply or withdraw electrons. It is the authors' belief that the single-molecule fluorescence approach can offer myriad possibilities to study nanoparticle catalysis at the single-particle single-turnover resolution. With the global initiative in energy research, of which nanocatalysis is an integral part, we can expect groundbreaking studies to emerge in the coming years.

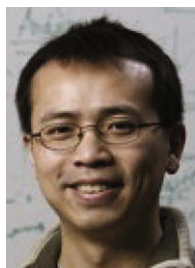
#### Acknowledgments

This work is supported in part by American Chemical Society Petroleum Research Foundation (47918-G5), NSF-funded Cornell Center for Materials Research (CCMR), and Cornell University. We thank Y.-T.E. Yeh and J.S. Kong for their contributions to the work and G. Liu for critical reading of the manuscript.

#### References

- [1] G.A. Somorjai, A.M. Contreras, M. Montano, R.M. Rioux, Proc. Natl. Acad. Sci. USA 103 (2006) 10577.
- [2] G. Ertl, H. Knözinger, J. Weitkamp, Handbook of Heterogeneous Catalysis, VCH, Weinheim, 1997.
- [3] A.T. Bell, Science 299 (2003) 1688.
- [4] C. Burda, X. Chen, R. Narayanan, M.A. El-Sayed, Chem. Rev. 105 (2005) 1025.
- [5] U. Heiz, U. Landman (Eds.), Nanocatalysis, Springer, Berlin, 2007.
- [6] G.C. Bond, C. Louis, D.T. Thompson (Eds.), Catalysis by Gold, Imperial College Press, London, 2006.
- [7] R.M. Crooks, M. Zhao, L. Sun, V. Chechik, L.K. Yeung, Acc. Chem. Res. 34 (2001) 181.
- [8] M. Chen, D.W. Goodman, Acc. Chem. Res. 39 (2006) 739.
- [9] M.D. Hughes et al., Nature 437 (2005) 1132.
- [10] Y. Sun, Y. Xia, Science 298 (2002) 2176.

- [11] H. Lee, S.E. Habas, S. Kwekskin, D. Butcher, G.A. Somorjai, P. Yang, *Angew. Chem. Int. Ed.* 45 (2006) 7824.
- [12] T.F. Jaramillo, K.P. Jorgensen, J. Bonde, J.H. Nielson, S. Horch, I. Chorkendorff, *Science* 317 (2007) 100.
- [13] Z.L. Wang, *Adv. Mater.* 15 (2003) 1497.
- [14] P.-L. Hansen, J.B. Wagner, S. Helveg, J.R. Rostrup-Nielsen, B.S. Clausen, H. Topsøe, *Science* 295 (2002) 2053.
- [15] M.A. Newton, C. Belver-Coldeira, A. Martinez-Arias, M. Fernandez-Garcia, *Nat. Mater.* 6 (2007) 528.
- [16] M. Haruta, N. Yamada, T. Kobayashi, S. Iijima, *J. Catal.* 115 (1989) 301.
- [17] Basic Energy Needs: Catalysis for Energy, Report from the U.S. Department of Energy Basic Energy Sciences Workshop, 2007.
- [18] P.D. Jadzinsky, G. Calero, C.J. Ackerson, D.A. Bushnell, R.D. Kornberg, *Science* 318 (2007) 430.
- [19] G.A. Somorjai, *Introduction to Surface Chemistry and Catalysis*, Wiley-Interscience, New York, 1994.
- [20] D.A. King, D.P. Woodruff (Eds.), *Phase Transitions and Adsorbate Restructuring at Metal Surfaces*, Elsevier Science, 1994.
- [21] N. Kruse, *Ultramicroscopy* 89 (2001) 51.
- [22] F. Tao et al., *Science* 322 (2008) 932.
- [23] P. Nolte, A. Stierle, N.Y. Jin-Phillipp, N. Kasper, T.U. Schulli, H. Dosch, *Science* 321 (2008) 1654.
- [24] E.d. Smit et al., *Nature* 456 (2008) 222.
- [25] F.-R.F. Fan, J. Kwak, A.J. Bard, *J. Am. Chem. Soc.* 118 (1996) 9669.
- [26] F.-R.F. Fan, A.J. Bard, *Science* 277 (1997) 1791.
- [27] J. Meier, K.A. Friedrich, U. Stimming, *Faraday Discuss.* 121 (2002) 365.
- [28] J. Meier, J. Schiötz, P. Liu, J.K. Nørskov, U. Stimming, *Chem. Phys. Lett.* 390 (2004) 440.
- [29] S. Chen, A. Kucernak, *J. Phys. Chem. B* 108 (2004) 13984.
- [30] D. Krapf, M.-Y. Wu, R.M.M. Smeets, H.W. Zandbergen, C. Dekker, S.G. Lemay, *Nano Lett.* 6 (2006) 105.
- [31] C. Novo, A.M. Funston, P. Mulvaney, *Nat. Nanotechnol.* 3 (2008) 598.
- [32] W. Xu, J.S. Kong, Y.-T.E. Yeh, P. Chen, *Nature Mater.* 7 (2008) 992.
- [33] W. Xu, J.S. Kong, P. Chen, *J. Phys. Chem. C* (2009), doi:10.1021/jp808240c.
- [34] W. Xu, J.S. Kong, P. Chen, *Phys. Chem. Chem. Phys.* (2009), doi:10.1039/B820052A.
- [35] L. Edman, Z. Fišlides-Papp, S. Wennmalm, R. Rigler, *Chem. Phys.* 247 (1999) 11.
- [36] K. Velonia et al., *Angew. Chem. Int. Ed.* 44 (2005) 560.
- [37] B.P. English et al., *Nat. Chem. Biol.* 3 (2006) 87.
- [38] R.D. Smiley, G.G. Hammes, *Chem. Rev.* 106 (2006) 3080.
- [39] M.B. Roeffaers, B.F. Sels, H. Uji-i, F.C. de Schryver, P.A. Jacobs, D.E. de Vos, J. Hofkens, *Nature* 439 (2006) 572.
- [40] D.A. Handley, in: M.A. Hayat (Ed.), *Colloidal Gold: Principles, Methods and Applications*, Academic Press, Inc., San Diego, 1989, p. 1.
- [41] D.A. Handley, in: M.A. Hayat (Ed.), *Colloidal Gold: Principles, Methods, and Applications*, Academic Press, Inc., San Diego, 1989, p. 13.
- [42] C.N. Satterfield, *Heterogeneous Catalysis in Practice*, McGraw-Hill Book Company, New York, 1980.
- [43] S.C. Kou, B.J. Cherayil, W. Min, B.P. English, X.S. Xie, *J. Phys. Chem. B* 109 (2005) 19068.
- [44] M.A. Newton, *Chem. Soc. Rev.* 37 (2008) 2644.
- [45] H.P. Lu, L.Y. Xun, X.S. Xie, *Science* 282 (1998) 1877.
- [46] J.B. Witkoskie, J. Cao, *J. Chem. Phys.* 121 (2004) 6361.
- [47] G.A. Somorjai, R.L. York, D. Butcher, J.Y. Park, *Phys. Chem. Chem. Phys.* 9 (2007) 3500.
- [48] G.A. Somorjai, J.Y. Park, *Chem. Soc. Rev.* 37 (2008) 2155.
- [49] M. Baumer, J. Libuda, K.M. Neyman, N. Rosch, G. Rupprechter, H.-J. Freund, *Phys. Chem. Chem. Phys.* 9 (2007) 3541.
- [50] M. Grzelczak, J. Pérez-Juste, P. Mulvaney, L.M. Liz-Marzán, *Chem. Soc. Rev.* 37 (2008) 1783.
- [51] T.K. Sau, C.J. Murphy, *J. Am. Chem. Soc.* 126 (2004) 8648.
- [52] A.R. Tao, S. Habas, P. Yang, *Small* 4 (2008) 310.
- [53] X.-M. Qian, S. Nie, *Chem. Soc. Rev.* 37 (2008) 912.
- [54] J. Kneipp, H. Kneipp, K. Kneipp, *Chem. Soc. Rev.* 37 (2008) 1052.
- [55] P.G. Etchegoin, E.C. Le Ru, *Phys. Chem. Chem. Phys.* 10 (2008) 6079.
- [56] L. Brus, *Acc. Chem. Res.* 41 (2008) 1742.



**Peng Chen** received his B.S. from Nanjing University, China in 1997. After spending a year at University of California at San Diego with Prof. Yitzhak Tor, he moved to Stanford University and did his Ph.D. with Prof. Edward Solomon in bioinorganic and physical inorganic chemistry. In 2004, he joined Prof. Sunney Xie's group at Harvard University for postdoctoral research in single-molecule biophysics. He started his assistant professorship at Cornell University in 2005. His current research interests focus on single-molecule imaging of bioinorganic chemistry and nanoscale catalysis. He has received a Camille and Henry Dreyfus New Faculty award and a NSF Career award.



**Weilin Xu** obtained his B.S. in chemistry at Jilin University, China in 2001, and his Ph.D. at Changchun Institute of Applied Chemistry, Chinese Academy of Sciences in 2006. He is currently a postdoctoral fellow in the Department of Chemistry and Chemical Biology at Cornell University, working on single-molecule catalysis of nanomaterials in Prof. Peng Chen's lab.



**Xiaochun Zhou** obtained his Ph.D. in Physical Chemistry at the Chinese Academy of Sciences in 2007. He is currently a postdoctoral fellow in the Department of Chemistry and Chemical Biology at Cornell University, working on single-nanoparticle catalysis in Prof. Peng Chen's lab.



**Debashis Panda** obtained his B.Sc. in chemistry from Calcutta University, India in 2002, and received his M.Sc. (2004) and Ph.D. (2007) from Indian Institute of Technology, Bombay. He is currently conducting his postdoctoral work on single-molecule protein-DNA interactions and nanocatalysis in Prof. Peng Chen's lab in the Department of Chemistry and Chemical Biology at Cornell University.



**Aleksandr Kalininskiy** just finished his B.S. in Biology at Cornell University. He is currently in the process of applying to graduate schools in the field of biomedical engineering.